The K-derived MLT sector geomagnetic indices

A. Chambodut, A. Marchaudon, Michel Menvielle, Farida El-Lemdani Mazouz, C. Lathuillére

The *K*-derived MLT sector geomagnetic indices

A. Chambodut,[1] A. Marchaudon,[2,3] M. Menvielle,[4,5]
F. El-Lemdani Mazouz,[4] and C. Lathuillère[6]

Received 28 June 2013; revised 4 September 2013; accepted 8 September 2013; published 19 September 2013.

[1] New subauroral *K*-derived sector indices are proposed. They are based on the *K* local geomagnetic activity indices from the planetary *am* network stations, and their derivation scheme draws directly from that of *am* indices. Four Magnetic Local Time (MLT) sectors are considered, leading to four different *K*-derived MLT sector indices: the $a\sigma_{\mathrm{Dawn}}$ (03–09 MLT), $a\sigma_{\mathrm{Noon}}$ (09–15 MLT), $a\sigma_{\mathrm{Dusk}}$ (15–21 MLT), and $a\sigma_{\mathrm{Midnight}}$ (21–03 MLT) indices. They cover more than four solar cycles and, thus, allow robust statistical analysis. Statistical studies of the whole $a\sigma$ data series and case studies for two geomagnetic storms are presented. These analyses clearly show that the four $a\sigma$ have specific behaviors and that it is possible to get insight into both the statistical properties of the physical processes responsible for the observed geomagnetic activity and contribution to the dynamics of a given storm.
Citation: Chambodut, A., A. Marchaudon, M. Menvielle, F. El-Lemdani Mazouz, and C. Lathuillère (2013), The *K*-derived MLT sector geomagnetic indices, *Geophys. Res. Lett.*, *40*, 4808–4812, doi:10.1002/grl.50947.

1. Introduction

[2] The *K* indices were the first magnetic indices providing a quantitative description of the magnetic activity. They were introduced at the end of the 1930s [*Bartels*, 1938]. *K* indices from network of observatories were then used to derive the so-called *K*-derived planetary geomagnetic indices that provide integrated and pertinent information about the Earth's magnetic activity variations [see *Mayaud*, 1980; *Menvielle and Berthelier*, 1991; *Menvielle et al.*, 2011, and references therein]. On a planetary scale, the *am* index is one of the most pertinent geomagnetic quantity to characterize the Earth's magnetosphere-ionosphere activity and its coupling with the solar wind [*Svalgaard*, 1977].

[3] A need for new indices providing a better spatial description of geomagnetic activity has progressively emerged. For internal field modeling [*Finlay et al.*, 2010], a more precise temporal and spatial monitoring of geomagnetic disturbances would greatly improve the selection of quiet time magnetic satellite data, as the external field spectrum overlaps partly with that of the internal field one [*Constable and Constable*, 2004]. Besides, space weather development resulted in a need for new indices describing more precisely the Earth's electrodynamics.

[4] *Menvielle and Paris* [2001] proposed up to five sector indices fixed in geographic longitude and based on *am* calculation and network. These sector longitudinal indices have proved good efficiency for selection of quiet time magnetic satellite data [*Thomson and Lesur*, 2007], but not for description of the different sources of Earth's magnetic activity, which are organized with respect to MLT. Other attempts to get a regional description of magnetic activity have been made. *Newell and Gjerloev* [2012] have proposed four sector indices fixed in Magnetic Local Time (MLT) and based on the *SYM-H* index calculation. They are mainly dedicated to the pattern characterization of the ring current that has large spatiotemporal variations. We propose four new subauroral sector indices defined with respect to MLT: the $a\sigma$ indices. They cover respectively the dawn (03–09 MLT), noon (09–15 MLT), dusk (15–21 MLT), and midnight (21–03 MLT) sectors.

[5] This paper is dedicated to the presentation of these four new indices and to a first illustration of their possible contribution to Earth's ionized environment studies. Section 2 presents the magnetic observatories network and the algorithm used to calculate these indices. Section 3 presents statistical UT/DOY (day of year) pattern of the $a\sigma$ indices obtained over more than four solar cycles, as well as their respective variations for different magnetic activity levels. Section 4 shows the behavior of the four $a\sigma$ during two magnetic storms. Section 5 is dedicated to discussion and conclusion.

2. Methodology

[6] The derivation scheme of the *K*-derived MLT sector indices draws directly from that of *am* indices available from 1959 onwards [*Mayaud*, 1980]. The *am* indices are computed from the *K* indices scaled at a network of magnetic observatories, the so-called *am* stations, located at latitudes close to 50° corrected geomagnetic latitudes, with relatively homogeneous distribution in longitude in each hemisphere (Figure 1). The *am* stations are gathered into five groups in the Northern Hemisphere (G1 to G5) and four in the Southern one after 1979 (G6 to G9), and only three before (G6 to G8).

[7] For each group i, the mean longitude ϕ_i of the magnetic observatories is calculated. For each 3 h interval, the *K* values measured at the observatories of one group are averaged leading to the $\overline{K_i}$ intermediate indices. The $\overline{K_i}$

[1]Université de Strasbourg, CNRS, Institut de Physique du Globe de Strasbourg, Strasbourg, France.
[2]Université de Toulouse, Toulouse, France.
[3]CNRS, IRAP, Toulouse, France.
[4]Université de Versailles St Quentin, CNRS, LATMOS, Guyancourt, France.
[5]Université de Paris-Sud, Orsay, France.
[6]Université Joseph Fourier, CNRS, IPAG, Grenoble, France.

Corresponding author: A. Chambodut, Institut de Physique du Globe de Strasbourg; UMR 7516, Université de Strasbourg/EOST, CNRS; 5 rue René Descartes F-67084 Strasbourg Cedex, France. (aude.chambodut@unistra.fr)

0094-8276/13/10.1002/grl.50947

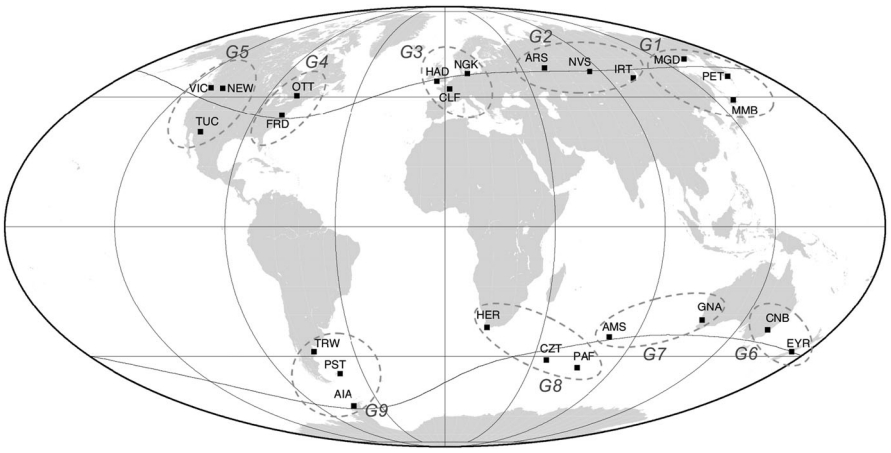

Figure 1. Stations and groups of the *am* network.

are converted back to amplitudes to obtain $\overline{a_i}$ indices, expressed in nT for each group (see *Menvielle et al.* [2011] for further explanation). For each 3 h interval, the $\overline{a_i}$ are linearly interpolated over each hemisphere independently for obtaining the curve $a(\phi)$ (see Figure 2) which is a first-order approximation of the variation with longitude of the intensity of the geomagnetic activity as described by *K* indices.

[8] Four MLT sectors are then defined, each 90° wide and fixed with regards to the Sun-Earth direction: dawn (03–09 MLT), noon (09–15 MLT), dusk (15–21 MLT), and midnight (21–03 MLT). Geomagnetic observatories are thus drifting over time and lie successively in the four MLT sectors. For each MLT sector and for each 3 h interval, the corresponding $a\sigma$ index is a mean between Northern and Southern values. Each hemispheric index is itself the average of $a(\phi)$ between the limits in longitude of the considered MLT sector *j*.

[9] This definition allows the derivation of homogeneous and continuous series of $a\sigma$ indices since the beginning of the *am* indices series, from 1959 onwards.

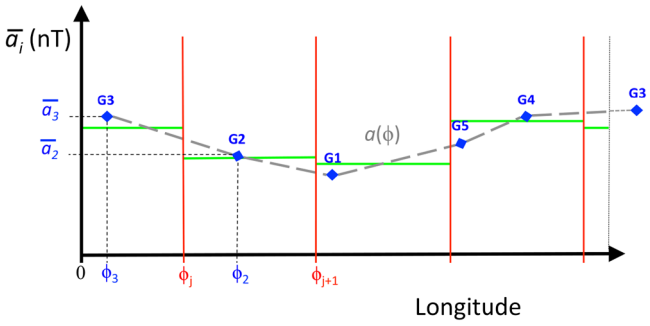

Figure 2. Methodology of $a\sigma_N$ Northern Hemispheric index calculation for a single 3 h interval: the five groups of longitude ϕ_i where $1 < i < 5$ with the corresponding $\overline{a_i}$ mean values calculated over the magnetic observatories of each group (blue diamonds), the interpolated curve $a(\phi)$ (broken gray curve), the MLT sectors (red vertical lines), and the $a\sigma_N$ hemispheric index of the considered MLT sector (green horizontal lines).

3. Statistical Behavior of the MLT Sector Indices

[10] The statistical results presented here cover the period 1959–2011, i.e., more than four solar cycles, and include consequently 53 years. For each 3 h UT interval, we calculate the four MLT sector indices which are then binned as a function of UT and DOY, leading to 53 values per bin. Finally, a running average over 11 days is performed in order to allow a better assessment of variations on the UT/DOY graphics. This average is not changing the seasonal variations, while allowing to smooth outliers values. The mean values in each bin are displayed as a function of UT and DOY in Figure 3 (first four colored panels). The DoY variations of the UT daily mean values of the four MLT sector indices are displayed in the fifth panel.

[11] The dusk and midnight sector patterns (Figure 3) display maxima around equinoxes, a minimum at 16:30 UT around the June solstice and at 04:30 UT around the December solstice. This pattern is also visible in the dawn and noon MLT sectors (Figure 3), albeit with smaller amplitude variations as well as smaller mean values. Such a complex UT/DOY pattern of Earth's magnetic activity has already been clearly identified in planetary indices such as *am* [*La Sayette and Berthelier*, 1996; *Cliver et al.*, 2000]. Although the cause of these variations is still under debate, a complex combination of three effects is generally invoked. The *axial effect* [e.g., *Hundhausen et al.*, 1971] is due to the varying angle between the Earth's orbit plane and the Sun's equatorial plane. As the Earth reaches higher solar latitudes, it encounters higher solar wind speed which enhances magnetic activity close to the equinoxes. The *Russell-McPherron effect* [*Russell and McPherron*, 1973] is due to the varying angle between the *z* axis in the geocentric solar magnetospheric (GSM) coordinate system and the Sun's equatorial plane. The Parker spiral displays a component along the *z* axis (parallel or antiparallel) in the Earth's GSM frame which maximizes around the equinoxes, favoring the Sun-Earth coupling through dayside magnetopause reconnection and substorm triggering. The *equinoctial effect* is due to the varying angle between the Earth-Sun's line and the Earth's dipole axis. The variations of this angle [e.g., *Cliver et al.*, 2000; *O'Brien and McPherron*, 2002; *Svalgaard*, 2011] very well reproduce the UT/DOY pattern presented here and confirm that the equinoctial effect is the main cause of the

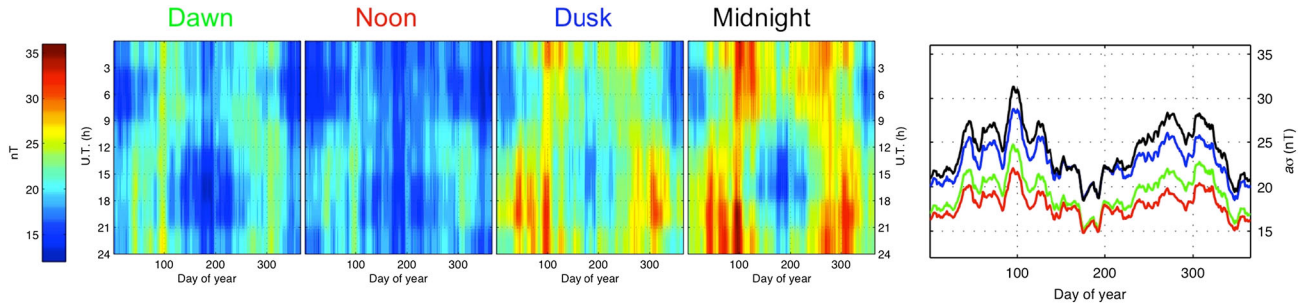

Figure 3. UT/DOY color pattern for the 4 MLT sector indices. The mean values over UT of these four indices plotted against DOY are displayed in the fifth panel. The color code in this panel corresponds to the one used for the names of the sectors above each color panel.

magnetic variability observed in each MLT sector. A variable magnetopause shape and cusp geometry is the most probable cause for it [*Crooker and Siscoe*, 1986]. Intensity differences from one sector to another are outlined in the fifth panel (Figure 3), which shows the UT daily mean of each of the four MLT sector indices. The seasonal behavior is very similar in all curves, and the amplitude level increases from noon over dawn and dusk to midnight. Local maxima in the semiannual variations, for example around the DOY 95, are observed which are due to the accumulation of storms during equinoctial periods over the averaged 53 year series [*Crooker et al.*, 1992].

[12] Figure 4 display the mean values of the MLT sector indices as a function of DOY for four geomagnetic activity classes (from left to right): intense activity ($am > 40$ nT), moderate activity (20 nT< $am < 40$ nT), quiet (10 nT< $am <$ 20 nT), and very quiet ($am < 10$ nT). The limits of am classes have been chosen in order to have about the same number of samples in each bin for the three lowest classes: moderate, quiet, and very quiet (104, 120, and 144 3 h values per DOY, respectively). For intense activity, i.e., the less populated class, the mean number of samples is only 56 per DOY.

[13] For the intense activity class, the behaviors of the four MLT sector indices mimic what is observed for the mean values (Figure 3, fifth panel and Figure 4, first panel). We observe here that the peak around day 200, i.e., during the solstice minimum, can be attributed to four super storms, including the one associated with the Bastille day solar storm of 14 July 2000 [*Clua de Gonzalez et al.*, 2002]. During solstices, the mean activity reaches a minimum and the number of samples per DOY accordingly decreases for the intense activity class. The presence of such superstorms thus strongly impacts on the mean activity value for the corresponding DOY. This is not the case when there are more samples per DOY (other activity classes) or during periods where mean activity is higher.

[14] In contrast, in the two classes corresponding to quiet and very quiet activity (Figure 4, third and fourth panels), the semiannual variation is maximum during solstices. This is due to solar illumination which is the dominating ionosphere behavior at low activity levels. For very quiet activity, all MLT sector indices have about the same mean values, apart from periods around the June solstice where the maximum is clearly more pronounced in the dusk sector, due to the delayed diurnal response of the neutral atmosphere. The exospheric temperature maximized post noon, causing atmospheric heating and expansion, and enhancements of magnetic activity through ions drag. This effect should also be seen in the December solstice, but it is not clear. This asymmetry may illustrate a possible influence of the scarce distribution of stations in the Southern Hemisphere. For quiet activity, the maxima at solstices begin to vanish particularly in the midnight sector where they almost disappear. In addition, the mean value shows a clear separation between dawn/noon on one hand and dusk/midnight on the other hand, which illustrates the intensification of the solar wind-magnetosphere coupling.

[15] Moderate activity shows a transition between the maxima at solstices and the equinoctial behavior at higher activity level. Indeed, the midnight and dawn sectors start to display the semiannual pattern with a maximum during equinoxes.

4. Geomagnetic Storms

[16] In order to highlight the interest of such MLT sector indices, this section presents two geomagnetic storms of the last solar cycle (29 May 2003 and 27 July 2004) exhibiting

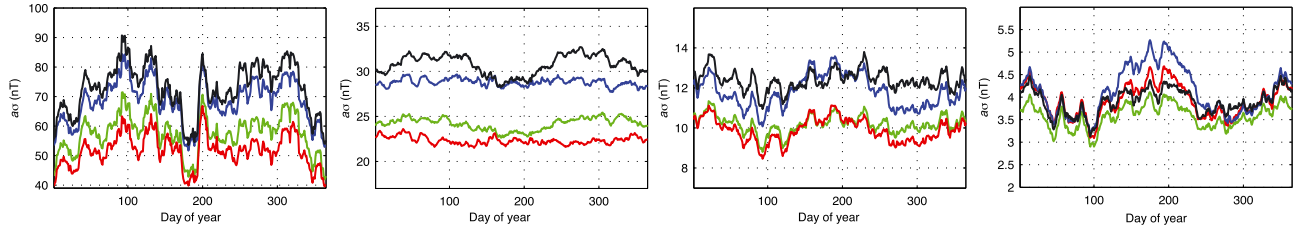

Figure 4. Comparison of the MLT sector indices separated in four activity classes, from left to right: $am > 40$ nT, 20 nT < $am < 40$ nT, 10 nT < $am < 20$ nT, and $am < 10$ nT. The color code is similar to that of Figure 3.

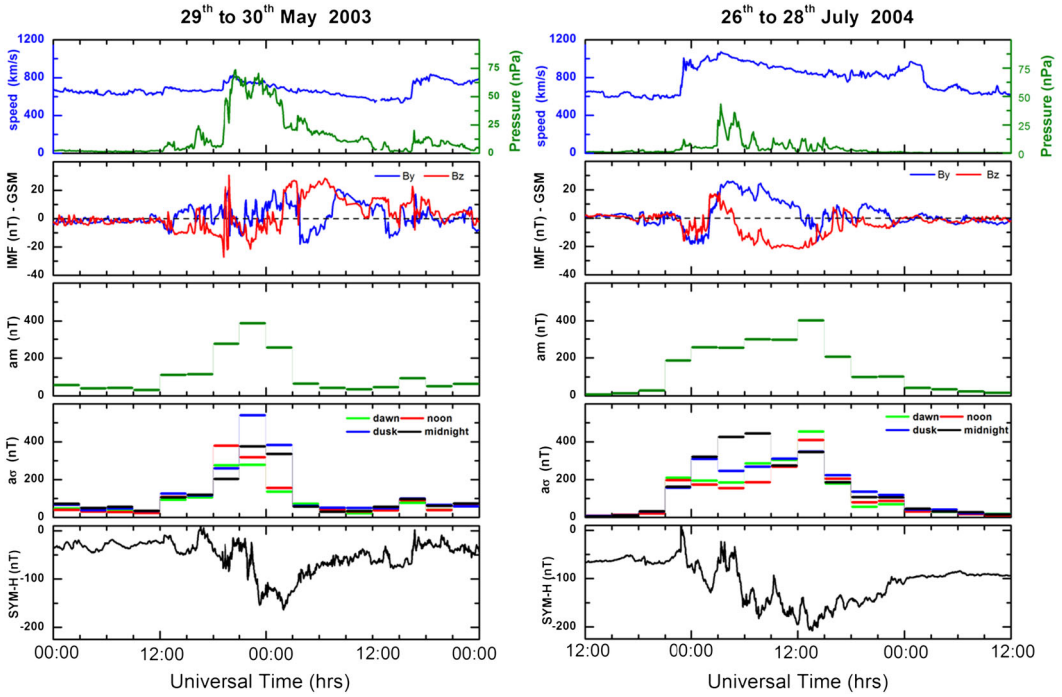

Figure 5. Solar wind parameters and geomagnetic indices during the (left) 29 May 2003 and (right) 27 July 2004 storms. (top to bottom) The solar wind pressure (green line) and velocity (blue line), the *Z* and *Y* components of the interplanetary magnetic field (IMF) in geocentric solar magnetospheric (GSM) coordinates (red and blue lines), the *am* index, the four MLT sector indices (with the color code defined in Figure 2), and the *SYM-H* index.

strong differences in each $a\sigma$ behavior (Figure 5). After describing quickly the main characteristics of the solar wind plasma and magnetic field, we will describe the evolution of the *am* and *SYM-H* indices, before looking at the $a\sigma$ variations. We will present rapidly the physical processes responsible for $a\sigma$ behaviors but without entering into details.

[17] The 29 May 2003 geomagnetic storm (Figure 5, left) was driven by three successive halo coronal mass ejections (CME), forming a large magnetic cloud with a globally southward then northward interplanetary magnetic field (IMF), accompanied by intense solar wind pressure pulses (up to 75 nPa) and interplanetary shocks [*Hanuise et al.*, 2006]. The storm lasts less than a day: with *am* showing a single peak about 400 nT around 22:00 UT (29 May) and *SYM-H* showing a complex main phase decreasing to –164 nT, followed by a smooth recovery phase. Looking at the MLT sector indices global profile, we observe two successive enhancements of all $a\sigma$ at 12:00 and 18:00 UT (29 May), the second being the strongest, until 03:00 UT (30 May) when all $a\sigma$ fall again to low background values, corresponding to the end of the storm main phase. From the second enhancement, the four $a\sigma$ start to show different behaviors. The $a\sigma_{\mathrm{Noon}}$ index shows first the highest value followed by a quick decrease. This strong $a\sigma_{\mathrm{Noon}}$ is caused by solar wind pressure enhancement and southward turning of the IMF, due to magnetosphere compression and enhanced dayside magnetopause reconnection, favoring dayside solar wind-magnetosphere coupling. The northward IMF turning can explain the strong decrease of $a\sigma_{\mathrm{Noon}}$ after 00:00 UT (30 May). Initially nearly identical, $a\sigma_{\mathrm{Dusk}}$ and $a\sigma_{\mathrm{Dawn}}$ start to depart around the time of storm maximum (21:00 UT, 29 May), as identified by *am* and *SYM-H*. This strong dawn-dusk asymmetry may be explained by partial ring current intensification [*Shi et al.*, 2005, 2008] and/or auroral electrojet asymmetry. Finally, $a\sigma_{\mathrm{Midnight}}$ and $a\sigma_{\mathrm{Dusk}}$ show the highest values after 21:00 UT (29 May), and could be explained by substorm current wedge and partial ring current intensifications as seen with the *ASYM – H* index (not shown).

[18] The 27 July 2004 geomagnetic storm (Figure 5, right) was driven by a sheath (Coronal Hole Stream) followed by a very fast magnetic cloud associated with a CME [*Kataoka and Miyoshi*, 2008] and was preceded by two other geomagnetic storms. In the cloud, the IMF shows a slow magnetic rotation with positive IMF-By and negative IMF-Bz. It is also characterized by a high pressure (20 nPa) and fast solar wind speed. This storm also lasts about a day, but the planetary *am* and *SYM-H* indices show more complex variations than the 29 May 2003 storm, *am* reaches intense values (> 200 nT) for more than half a day, the *SYM-H* index shows successive declining and partial recovery phases. Looking at the MLT sector indices global profile, we observe strong activity of all $a\sigma$ throughout the course of the main and recovery phases of the storm but with variable intensities. The $a\sigma_{\mathrm{Noon}}$ index shows relatively high values throughout the storm duration. This can be explained by the strong and long southward IMF periods during the sheath and the magnetic cloud and the numerous solar wind pressure pulses, enhancing dayside solar wind-magnetosphere coupling. Throughout the storm, $a\sigma_{\mathrm{Dusk}}$ shows similar or slightly higher values than $a\sigma_{\mathrm{Dawn}}$, consistent with dusk partial ring current intensification. We can however note that $a\sigma_{\mathrm{Dawn}}$ dominates the 3 h interval associated with storm maximum (12:00 UT, 27 July) and is caused by three successive strong intensifications of the westward (dawn) electrojet, as seen

with the *AL* index (not shown). Finally, $a\sigma_{\text{Midnight}}$ dominates the first part of the storm (00:00–09:00 UT, 27 July), with high values (> 400 nT), implying strong substorm activity driven by the southward IMF in the magnetic cloud.

[19] A more detailed study of the behavior of the MLT sector indices is outside the scope of this paper, but through these two storm examples, we have shown the ability of these indices to describe more precisely the complex regional electrodynamics of the magnetosphere-ionosphere system driven by solar wind interaction.

5. Discussion and Conclusion

[20] In this paper, we have presented to both the internal and the space weather community new geomagnetic indices with MLT sector dependencies: the *K*-derived MLT sector indices.

[21] Besides being the very first MLT sector indices, the $a\sigma$ are calculated in an easy and reproductive way on a well-known set of geomagnetic observatories. They cover more than four solar cycles and thus allow robust statistical analyses.

[22] Both statistical and geomagnetic storm studies have clearly shown the different behaviors of the four $a\sigma$. In particular, with only two storm examples, we have already been able to dissociate the effect linked to the dayside coupling (magnetopause reconnection and pressure pulse) from the one associated with substorm and partial ring current intensifications in the night and dusk sectors.

[23] Such indices however present also some drawbacks, essentially due to the limited spatial and temporal resolution of the available data set. Indeed, the network of magnetic stations is scarce in the Southern Hemisphere (see Figure 1). The use of *K* indices from groups of stations separated in longitude by more than 50° (i.e., about 4 MLT hours) may smooth the real geophysical variations in intensity as also does the 3 h temporal resolution.

[24] To overcome these drawbacks, we plan to develop new indices with better temporal resolution based on an extended observatories network. This is now possible thanks to the enhancement of the number of stations in both hemispheres (beginning of 21st century); however, such new indices can not be derived further back in the past.

[25] Despite their limitations, the $a\sigma$ indices will be useful in various direct, internal and external, applications such as: selection of magnetic satellite data for main field modeling, choice of active periods for magnetotelluric studies, space weather applications, etc. These indices are available and may be downloaded at the following web address: http://cdg.u-strasbg.fr/PortailEOST/Mag/ObsMag-data.html.

[26] **Acknowledgments.** We acknowledge the institutes, who operate the observatories and produce the *K* indices, and the use of geomagnetic indices data from ISGI Website (http://isgi.cetp.ipsl.fr). This study received funding from the European Community Seventh Framework Program (FP7-SPACE-2010-1) under the grant agreement 261948 (ATMOP project, http://www.atmop.eu). We would like to thank the two anonymous reviewers for their suggestions and comments.

[27] The Editor thanks two anonymous reviewers for their assistance in evaluating this paper.

References

Bartels, J. (1938), Potsdamer erdmagnetische Kennziffern, 1 Mitteilung, *Z. Geophys.*, *14*, 68–78.

Cliver, E. W., Y. Kamide, and A. G. Ling (2000), Mountains versus valleys: Semiannual variation of geomagnetic activity, *J. Geophys. Res.*, *105*(A2), 2413–2424, doi:10.1029/1999JA900439.

Clua de Gonzalez, A. L., V. M. Silbergleit, W. D. Gonzalez, and B. T. Tsurutani (2002), Irregularities in the semi-annual variations of the geomagnetic activity, *Adv. Space Res.*, *30*(140), 2215–2218.

Constable, C. G., and S. C. Constable (2004), Satellite magnetic field measurements: Applications in studying the deep earth, in *The State of the Planet: Frontiers and Challenges in Geophysics*, edited by R. S. J. Sparks, and C. J. Hawkesworth, pp. 147–160., AGU, Washington D. C.

Crooker, N. U., and G. L. Siscoe (1986), On the limits of energy transfer through dayside merging, *J. Geophys. Res.*, *91*, 13,393–13,397.

Crooker, N. U., E. W. Cliver, and B. T. Tsurutani (1992), The semiannual variation of great geomagnetic storms and the postshock Russell-McPherron effect preceding coronal mass ejecta, *Geophys. Res. Lett.*, *19*, 429–432.

Finlay, C. C., et al. (2010), International geomagnetic reference field: The eleventh generation, *Geophys. J. Int.*, *183*, 1216–1230, doi:10.1111/j.1365-246X.2010.04804.x.

Hanuise, C., et al. (2006), From the Sun to the Earth: Impact of the 27–28 May 2003 solar events on the magnetosphere, ionosphere and thermosphere, *Ann. Geophys.*, *24*, 129–151.

Hundhausen, A. J., S. J. Bame, and M. D. Montgomery (1971), Variations of solar-wind plasma properties: Vela observations of a possible heliographic latitude-dependence, *J. Geophys. Res.*, *76*, 5145–5154.

Kataoka, R., and Y. Miyoshi (2008), Average profiles of the solar wind and outer radiation belt during the extreme flux enhancement of relativistic electrons at geosynchronous orbit, *Ann. Geophys.*, *26*, 1335–1339.

La Sayette, P., and A. Berthelier (1996), The *am* annual-diurnal variations 1959-1988: A 30-year evaluation, *J. Geophys. Res.*, *101*, 10,653–10,663.

Mayaud, P. N. (1980), *Derivation, Meaning, and Use of Geomagnetic Indices, Geophysical Monograph 22*, AGU, Washington, D. C.

Menvielle, M., and A. Berthelier (1991), The *K*-derived planetary indices: Description and availability, *Rev. Geophys.*, *29*(3), 415–432, doi:10.1029/91RG00994.

Menvielle, M., and J. Paris (2001), The $a\lambda$ longitude sector geomagnetic indices, *Contrib. Geophys. Geod.*, *31*, 315–322.

Menvielle, M., T. Iyemori, A. Marchaudon, and M. Nose (2011), Geomagnetic indices, in *Geomagnetic Observations and Models*, edited by M. Mandea M. Korte, IAGA Special Sopron Book Series 5, Springer, Dordrecht, Heidelberg, London, New York. doi:10.1007/978-90-481-9858-08.

Newell, P. T., and J. W. Gjerloev (2012), SuperMAG-based partial ring current indices, *J. Geophys. Res.*, *117*, A05215, doi:10.1029/2012JA017586.

O'Brien, T. P., and R. L. McPherron (2002), Seasonal and diurnal variation of Dst dynamics, *J. Geophys. Res.*, *107*(A11), 1341, doi:10.1029/2002JA009435.

Russell, C. T., and R. L. McPherron (1973), Semi-annual variation of geomagnetic activity, *J. Geophys. Res.*, *78*, 92.

Shi, Y., E. Zesta, L. R. Lyons, A. Boudouridis, K. Yumoto, and K. Kitamura (2005), Effect of solar wind pressure enhancements on the storm time ring current asymmetry, *J. Geophys. Res.*, *110*, A10205, doi:10.1029/2005JA011019.

Shi, Y., E. Zesta, and L. R. Lyons (2008), Modeling magnetospheric current response to solar wind dynamic pressure enhancements during magnetic storms: 2. Application to different storm phases, *J. Geophys. Res.*, *113*, A10219, doi:10.1029/2008JA013420.

Svalgaard, L. (1977), Geomagnetic activity: Dependence on solar wind parameters, in *Skylab Workshop Monograph on Coronal Holes*, edited by J. B. Zirker, chap. 9, p. 371, Columbia Univ. Press, New York.

Svalgaard, L. (2011), Geomagnetic semiannual variation is not overestimated and is not an artifact of systematic solar hemispheric asymmetry, *Geophys. Res. Lett.*, *38*, L16107, doi:10.1029/2011GL048616.

Thomson, A., and V. Lesur (2007), An improved geomagnetic data selection algorithm for global geomagnetic field modelling, *Geophys. J. Int.*, *169*, 951–963, doi:10.1111/j.1365-246X.2007.03354.x